Journal of
Marine Science and Engineering

MDPI

Article

Influence of Foundation–Soil–Foundation Interaction on the Dynamic Response of Offshore Wind Turbine Jackets Founded on Buckets

Carlos Romero-Sánchez *, Jacob D. R. Bordón and Luis A. Padrón

University Institute of Intelligent Systems and Numerical Applications in Engineering, Universidad de Las Palmas de Gran Canaria, 35017 Las Palmas de Gran Canaria, Spain; jacobdavid.rodriguezbordon@ulpgc.es (J.D.R.B.); luis.padron@ulpgc.es (L.A.P.)
* Correspondence: carlos.romero@ulpgc.es

Abstract: This study investigates the impact of soil–structure interaction (SSI) and foundation–soil–foundation interaction (FSFI) on the dynamic behaviour of jacket substructures founded on buckets for offshore wind turbines. A parametric analysis was conducted, focusing on critical load cases for conservative foundation design. Different load configurations were examined: collinear wind and wave (fluid–structure interaction) loads, along with misaligned configurations at 45° and 90°, to assess the impact of different loading directions. The dynamic response was evaluated through key structural parameters, including axial forces, shear forces, bending moments, and stresses on the jacket. Simulations employed the National Renewable Energy Laboratory (NREL) 5MW offshore wind turbine mounted on the OC4 project jacket founded on suction buckets. An additional optimised jacket design was also studied for comparison. An OpenFAST model incorporating SSI and FSFI considering a homogeneous soil profile was employed for the dynamic analysis. The results highlight the significant role of the FSFI on the dynamic behaviour of multi-supported jacket substructure, affecting the natural frequency, acceleration responses, and internal forces.

Keywords: offshore wind turbines; jacket; bucket foundations; suction caisson; soil–structure interaction; foundation–soil–foundation interaction; OpenFAST; structural response

Citation: Romero-Sánchez, C.; Bordón, J.D.R.; Padrón, L.A. Influence of Foundation–Soil–Foundation Interaction on the Dynamic Response of Offshore Wind Turbine Jackets Founded on Buckets. *J. Mar. Sci. Eng.* **2024**, *12*, 2089. https://doi.org/10.3390/jmse12112089

Received: 29 October 2024
Revised: 13 November 2024
Accepted: 17 November 2024
Published: 19 November 2024

1. Introduction

In recent years, offshore wind energy has emerged as a crucial element in the expansion of renewable energy around the globe. Nowadays, most offshore wind turbines (OWTs) are installed in regions where sea depths allow for fixed-base units. Among these installations, monopiles constitute the most widely used substructure [1]. Nevertheless, the increasing deployment of wind farms in deeper waters has driven a significant rise in the adoption of multi-support substructures, such as jackets and tripods supported on piles or suctions caissons [2].

Determining the natural frequency of an offshore wind turbine is a critical aspect of the design process, as it helps to avoid resonance phenomena that could lead to structural failure or long-term deterioration due to fatigue. Consequently, it is essential to ensure that the system's fundamental frequency does not coincide with the rotor's operational speed range (1P) or the rotor blades' transition frequency (3P). Various studies have examined the influence of soil–structure interaction (SSI) on the natural frequencies of offshore wind turbines supported by monopiles [3–7] and jacket substructures [8–10], with significant effects observed.

The influence of SSI on the natural frequencies can be determined by using a complete soil–foundation–structure model, or by including the dynamic stiffnesses of the soil–foundation subsystem in the superstructure model. In order to determine the static

and dynamic stiffnesses, researchers have traditionally employed analytical methods applied to fundamental problems, such as the widely studied circular footing, which often yield closed-form solutions or methodologies that are both simple and of considerable practical utility, offering valuable physical insight [11,12]. While numerical methods like the Finite Element Method (FEM) and the Boundary Element Method (BEM) enable the analysis of more complex, general problems [13–15], the development of such models requires significant expertise and can be time-intensive. A relevant case is the application of this methodology to the calculation of stiffnesses and impedances of bucket foundations (see e.g., [16–19]). Consequently, considerable effort has been directed towards deriving closed-form expressions and stiffness charts based on numerical results. Some of these results [20,21] have been incorporated into various design codes, including the offshore standard DNV-OS-J101 [22].

Conversely, in comparison to the study of isolated foundations, the topic of the interaction between foundations has garnered less attention [23–27]. Some authors explore the dynamic interaction between rigid foundations on viscoelastic soils, using a 3D Boundary Element Method (BEM) and focusing on foundation–soil–foundation interaction (FSFI) [28–31], i.e., the effects of interaction through the soil between two or more foundations. This interaction results in a change in the stiffness of each element within the group when compared to the corresponding stiffness of the single foundation.

Thus, the volume of research focused on analysing the dynamic behaviour of OWT jackets founded on buckets including FSFI (or group effect) is small when compared with the number of studies conducted on monopod suction caissons. Furthermore, there is a significantly greater body of literature addressing jackets on piles compared to jackets on bucket foundations. For jackets on piles, SSI is typically modelled using approaches such as linear or nonlinear springs and dashpots [12,32–36]. In all of these studies, the dynamic characteristics of the foundation are critical to the overall dynamic response of the support structure. However, research focusing on jackets supported by suction caissons remains limited [16,37–43], despite their widespread use in current projects. Bhattacharya et al. [37] demonstrated that the fundamental eigenfrequency of vibration for offshore wind turbines (OWTs) supported by multiple shallow foundations (e.g., jackets mounted on three or four suction caissons) is primarily associated with low-frequency rocking modes of vibration about the principal axes. Jalbi et al. [38] demonstrated that a low vertical foundation stiffness, coupled with a low aspect ratio, facilitates the onset of a rocking mode of vibration in jacket-supported offshore wind turbines. Additionally, Cheng et al. [41] investigated the dynamic behaviour of the jacket structure under varying wind and wave directions, revealing that the parked mode significantly influenced the calculated fragilities associated with critical damage conditions in both the tower and the jacket structure. A contribution to the field of buckets is the work of Bordón et al. [44]. The authors propose a methodology for incorporating the foundation–soil–foundation interaction effects into the stiffness matrices of foundations of shallow and bucket foundations, and demonstrate its influence on the natural frequencies and stiffness of a jacket structure.

Several of the aforementioned studies primarily focus on the structural properties of OWTs using simplified models. However, the dynamic properties of these support structures play a crucial role in the system's design, and the distinctive characteristics of the OWTs including the specific nature of loads, the system's variable geometry due to blade rotation, and the continuous influence of the control system, suggest that specific tools, able to adequately model the various subsystems, should be used in structural and dynamic response analyses. For this reason, many authors analyse the dynamic response of OWTs by considering the combined effects of aerodynamic and wave loadings [45–48]. Time-domain analyses, incorporating nonlinear aero-hydro-servo-elastic simulations [32,34,35,49], are essential for accurately capturing the turbine's dynamic behaviour across different operational modes.

Thus, the review of the existing literature highlights the significant influence of SSI on the dynamic response of OWT jackets founded on buckets. Additionally, it highlights

the importance of considering various operating modes and the misalignment between wind and wave directions in assessing the dynamic behaviour of substructures. As a continuation in this line of research, this study evaluates the influence of the foundation–soil–foundation interaction on the dynamic response of jacket substructures for OWTs, founded on suction buckets. To do so, time-domain coupled analysis in OpenFAST will be used. Specifically, the paper analyses the structural response of the OC4 project four-legged jacket substructure for the NREL 5MW OWT subjected to different design load cases. The results obtained for an optimised jacket substructure are also presented.

2. Problem Definition

2.1. Offshore Wind Turbine Properties

The NREL 5 MW three-bladed turbine [50] is employed in this study. The main parameters of the OWT are given in Table 1. The support structure considered is the jacket support substructure designed for the phase I of the OC4 project, described by Vorpahl et al. [51]. Figure 1 provides an illustration of the main characteristics of the jacket structure for the OWT and Figure 2 details the geometry of the jacket. The properties of the steel material are as follows: shear modulus 80.8 GPa, Young's modulus 210 GPa, mass density 7850 kg/m^3, and damping ratio 2%. Bucket foundations are considered, with the characteristics provided by Salem et al. [52] for this structure. Thus, a diameter of 4.0 m and length of 4.0 m are considered. A homogeneous linear elastic half-space with a Poisson's ratio $\nu = 0.28$ and shear modulus $\mu = 15.625$ MPa is assumed.

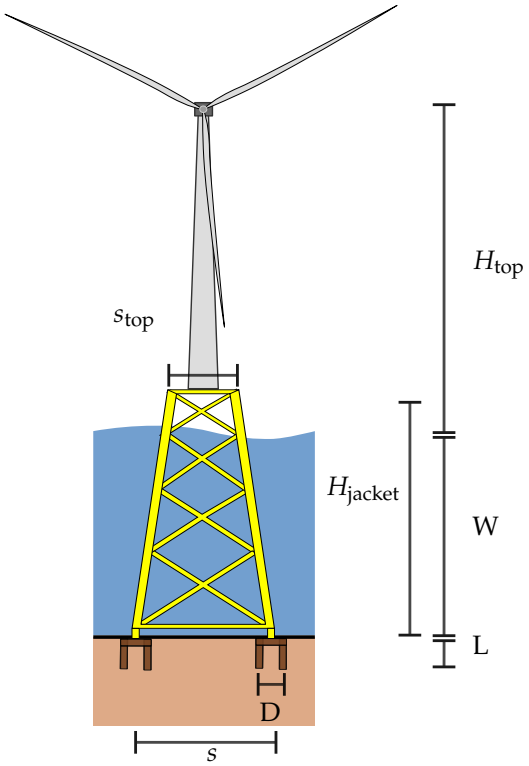

Figure 1. Representation of the NREL 5MW OWT mounted on a jacket founded on buckets.

Table 1. Key parameters of the offshore wind turbine.

Parameter	Value
Rotor diameter [m]	126
RNA mass [ton]	350
Rated wind speed [m/s] (V_r)	11.4
Hub height [m]	90.55
Tower top height from mean sea level [m] (H_{top})	88.15
Tower base height from mean sea level [m]	20.15

Table 1. *Cont.*

Parameter	Value
Thickness at the top of the tower [m]	30
Thickness at the tower base [m]	32
Tower top diameter [m]	4.00
Tower base diameter [m]	5.60
Water depth [m] (W)	50.00
Jacket height [m] (H_{jacket})	70.15
Top leg spacing [m] (s_{top})	8.00
Base leg spacing [m] (s)	12.00
Number of bracing levels	4
Number of legs	4

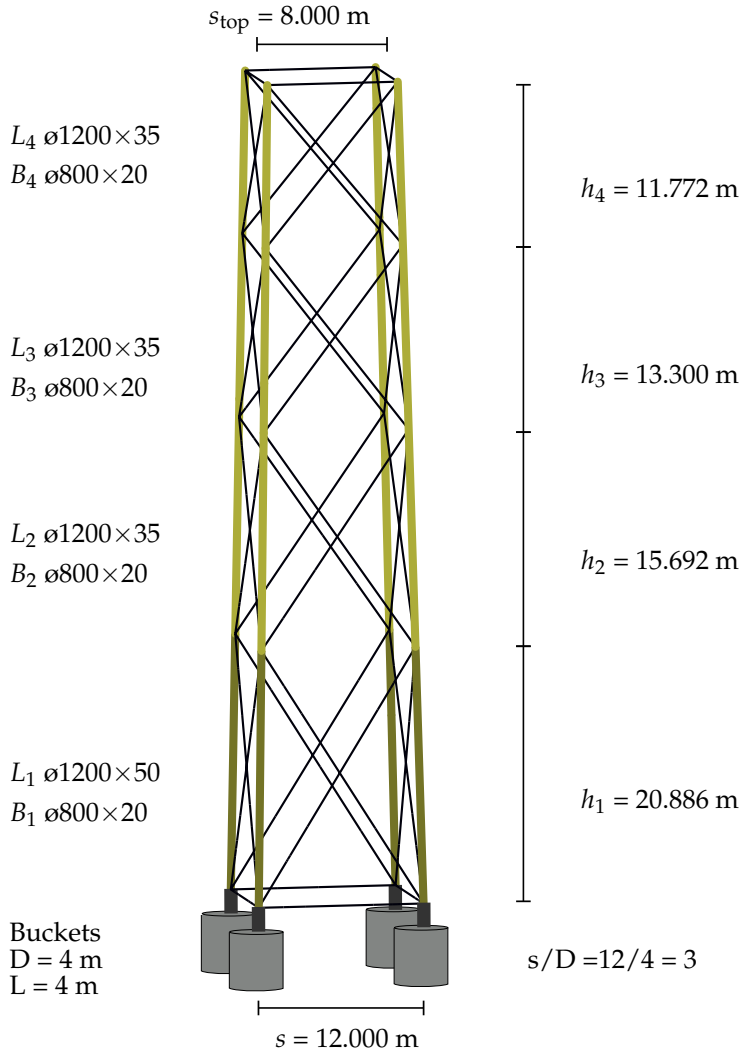

Figure 2. Geometry of the OC4 jacket with buckets. The diameter and thickness of each leg level L_i and bracings B_i are provided at the left of the figure in millimetres.

2.2. Load Cases

Wind turbines are exposed structures that must withstand a range of external influences, with the ability to operate under medium to high wind speeds being a fundamental requirement. Factors such as steady winds and turbulence serve as significant contributors to the overall loading experienced by wind turbines. The load analysis entails assessing the structural integrity of the system by evaluating a set of design load cases (DLCs). These DLCs are established in accordance with guidelines set by DNV [53].

Typically, design codes [53,54] describe hundreds of load cases for the design of offshore wind turbines, aimed at ensuring a service life of 25–30 years. However, not all these cases are pertinent to foundation design. For this study, the load cases outlined in Table 2 have been identified as the most relevant for performing a conservative analysis of the foundations, as described in Jalbi et al. [55] for jacket structures.

Table 2. Load scenarios.

SSI	**Fixed Base**	**SSI without FSFI**	**SSI with FSFI**
Operational Modes	**Power Production**	**Parked Mode**	
ID	**Case**	**Wind Model**	**Wave Model**
E-1	Normal Operational Conditions	Normal Turbulence Model (NTM) at the rated wind speed (V_r)	1-Year Extreme Sea States (ESS)
E-2	Extreme Wave Load Scenario	Extreme Turbulence Model (ETM) at the rated wind speed (V_r)	50-Year Extreme Wave Height (EWH)
E-3	Extreme Wind Load Scenario	Extreme Operating Gust (EOG) at the rated wind speed (V_r)	1-Year Extreme Wave Height (EWH)
Collinear 0° (C0)	Misalignment 90° (M90)	Misalignment 45° (M45)	Collinear 45° (C45)

The wind farm is situated at a location on the boundary waters between Dutch and British, with an average water depth of 50 m. Metocean conditions for this site are publicly accessible through the Dutch National Institute for Coastal and Marine Management. Extreme sea conditions, including Extreme Sea States (ESS) and Extreme Wave Height (EWH), are calculated as defined by DNVGL-ST-0437 [53], which classifies them into different categories based on wave height and frequency over specific periods. One-Year ESS and One-Year EWH correspond to extreme waves within a 1 year return period, with ESS determined by the average significant wave height ($H_{S,1}$) and EWH by the maximum recorded wave height ($H_{m,1}$). Similarly, 50-Year models pertain to a 50 year return period, where 50-year EWH is based on the Extreme Wave Height ($H_{m,50}$).

A summary of the metocean data is provided in Table 3. The wave loads in OpenFAST are computed through the module HydroDyn, where the wave kinematics model is chosen and defined. For the irregular waves, the JONSWAP spectrum was used since the sea state is considered developing when there are high wind speeds blowing on the wind turbine. The significant wave height and spectral wave period were detailed in accordance with the specified load case.

Table 3. Metocean data.

Parameter	**Value**
1-Year Significant Wave Height ($H_{S,1}$) [m]	6.6
1-Year Significant Wave Period ($T_{S,1}$) [s]	9.1
1-Year Maximum Wave Height ($H_{m,1}$) [m]	8.27
1-Year Maximum Wave Period ($T_{m,1}$) [s]	10.97
50-Year Maximum Wave Height ($H_{m,50}$) [m]	15.33
50-Year Maximum Wave Period ($T_{m,50}$) [s]	13.86

The turbulent wind fields, following the Kaimal spectrum, are generated in TurbSim for a hub-height mean wind speed of V_r = 11.4 m/s. This includes simulations under the Normal Turbulence Model (NTM), Extreme Turbulence Model (ETM), and Extreme Operating Gust (EOG), as well as Category B turbulent wind conditions [54]. The aerodynamic

forces acting on the blades and tower are calculated using the Blade Element Mode theory through the AeroDyn module.

The impacts of the operational modes and of the directionality of the loads on the jacket substructure have been previously analysed and discussed in [56]. The authors concluded that load combinations involving aligned wind and ground motion directions do not necessarily represent the worst-case scenario. The dynamic behaviour of the jacket, considering both wind and wave directions, was investigated by Cheng et al. [41], and they highlight the significant role of considering the parked mode in the computed fragilities of severe damage states for the tower and jacket structure. This effect is attributed to the increased aerodynamic damping, which helps mitigate the magnitude of vibrations induced by wind loads [32,57]. The analysis of the previous studies highlighted above reveals a clear influence of different operating modes and the misalignment between wave and wind directions on the dynamic response of the jacket.

In this paper, the dynamic response of the OWT is studied for two different operational modes: power production and parked modes, to compare the influence of the working conditions on the internal forces at the jacket substructure, considering bucket foundations. In addition, four potential loading scenarios can be considered: (C0) wind and wave loads are collinear, (M90) wind and wave loads are misaligned by 90°, (M45) wind and wave loads are misaligned by 45°, and (C45) wind and wave loads act at 45° relative to the structure. The hub is consistently oriented in the wind direction. Each of these scenarios must be evaluated against the load cases presented in Table 2. Figure 3 shows a graphical overview of the different load combinations used in the analysis.

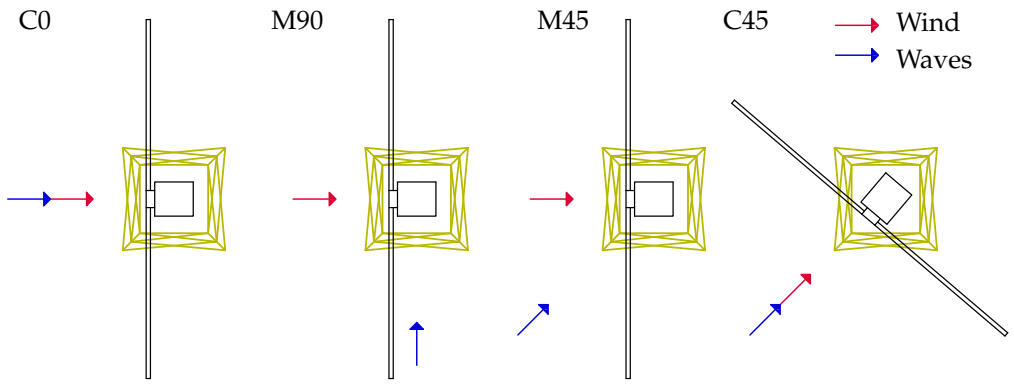

Figure 3. Plan view illustrating the loading direction on the OWT.

The analysis comprised a total of 144 distinct simulations. Each simulation lasted for 400 s, and the analysis was initiated at 150 s to mitigate the influence of the primary transient behaviour of the system. All load case combinations were simulated under three different conditions: fixed-based (No SSI), taking into account the foundation–soil–foundation interaction (SSI with FSFI), and considering the SSI using the corresponding stiffnesses to the single foundations without considering FSFI (SSI without FSFI).

3. Methodology

The incorporation of bucket–soil–bucket interaction effects into an OpenFAST model of a jacket-supported OWT requires the use of a model of this phenomenon formulated in such a way that it is compatible with the OpenFAST framework, without adding excessive complexity. With this idea in mind, bucket–soil–bucket interaction effects are herein incorporated through the alteration of the stiffness functions that define the response of each individual foundation. Such expressions are provided in closed-form format by Bordón et al. [44]. At the same time, and in order to be able to incorporate this information into OpenFAST, the SubDyn module was modified with the introduction of a stiffness matrix to represent the bucket foundations embedded in the homogeneous soils and with the ability to consider the foundation–soil–foundation interaction in multi-supported

structures. The OpenFAST model is employed to simulate the dynamic response of the OWTs considering different load cases. The primary practical contribution lies in its application to the time-domain analysis of polygonal configurations of multi-bucket jacket foundations for OWTs.

3.1. Soil–Structure Interaction

The formulation of a closed-form static stiffness matrix for bucket foundations and a set of formulas for correcting the stiffnesses obtained from single-foundation formulation are proposed by Bordón et al. [44,58]. A rigorous numerical model based on the Boundary Element Method (BEM) [17] is used to compute the stiffnesses of single foundations, and foundations as part of a group acting in a particular mode (vertical, horizontal, rocking, and torsion). The primary components consist of the stiffness parameters for the single foundation and the Green's function, which relates to the applied loads (including point forces and moments) and the observed responses (such as displacements and rotations) at the free surface.

These stiffness matrices can be readily incorporated into a superstructure finite element model to account for soil–structure interaction, including foundation–soil–foundation effects.

3.1.1. Simplified Stiffness Matrix

The stiffness matrix is derived in closed form from existing results pertaining to single foundations. The stiffness matrix attached to each jacket leg contains the six degrees of freedom and can be written as follows:

$$\mathbf{K}_0^{\text{no-int}} = \begin{bmatrix} K_H & 0 & 0 & 0 & -K_{SR} & 0 \\ 0 & K_H & 0 & K_{SR} & 0 & 0 \\ 0 & 0 & K_V & 0 & 0 & 0 \\ 0 & K_{SR} & 0 & K_{SR} & 0 & 0 \\ -K_{SR} & 0 & 0 & 0 & K_R & 0 \\ 0 & 0 & 0 & 0 & 0 & K_{KT} \end{bmatrix} \tag{1}$$

where K_H, K_V, K_R, K_{SR}, and K_T are the horizontal, vertical, rocking, coupled sway-rocking, and torsional stiffnesses. Specifically, the closed-form formulas for stiffness of rigid cylindrical foundations in homogeneous linear elastic half-space with depth L ($0 \leq L/D \leq 6$) and diameter D, perfectly bonded to the surrounding homogeneous soil with Poisson's ratio (ν) ($0 \leq \nu \leq 0.5$) and shear modulus μ, are employed in the present study. These formulas were derived for single foundations, which were used to fit enriched equations similar to those presented by Gazetas [20] and Wolf [59], leading to the following expressions:

$$K_V = \frac{2\mu D \ln(3-4\nu)}{1-2\nu}\left[1 + 1.08(1-0.76\nu)\left(\frac{L}{D}\right)^{0.82}\right] \tag{2}$$

$$K_H = \frac{4\mu D}{2-\nu}\left[1 + 1.85\left(\frac{L}{D}\right)^{0.75}\right] \tag{3}$$

$$K_R = \frac{\mu D^3}{3(1-v)}\left[1 + 7.7(1-1.2\nu)\left(\frac{L}{D}\right) + 10(1-0.7\nu)\left(\frac{L}{D}\right)^{2.5}\right] \tag{4}$$

$$K_{SR} = \frac{11\mu D^2}{4(15-17v)}\left[1 - 2\nu + 9.7(1-1.13\nu)\left(\frac{L}{D}\right) + 11.2(1-0.82\nu)\left(\frac{L}{D}\right)^{1.75}\right] \tag{5}$$

$$K_T = \frac{2\mu D^3}{3}\left[1 + 5.26\left(\frac{L}{D}\right)^{0.93}\right] \tag{6}$$

3.1.2. Foundation–Soil–Foundation Interaction

A practical way of incorporating the foundation–soil–foundation interaction into the computation of the stiffness of multi-bucket foundations is presented in [44], introducing a

set of closed-form correction factors to the common simplified stiffness matrix built from the already known stiffnesses of individual single buckets. The closed-form formulae were obtained for tripod and tetrapod arrangements of buckets in homogeneous and non-homogeneous soils.

Group effects are sensitive mainly to spacing ($\tilde{s} = s/D$), Poisson's ratio (ν), foundation shape ratio (L/D), diameter (D), and the number of foundations (N = 4). To quantify the magnitude of the foundation–soil–foundation interaction within the entire foundation system, the following group effect stiffness correction factors can be defined:

$$\gamma_{[\,]} = \frac{K_{[\,]}^{\mathrm{FSFI}}}{K_{[\,]}} \tag{7}$$

where the subindex [ ] = H,V,R,SR,T denotes any of the stiffness components. They relate stiffnesses including interaction and stiffnesses not including it. These group effect stiffness correction factors for multi-bucket foundations in homogeneous soil for tetrapod arrangements are approximated as follows:

$$\gamma_V = \frac{1}{1 + ((1-\nu)(1+\sqrt{2}/4)k_V)/\tilde{s}} \tag{8}$$

$$\gamma_H = \frac{1 + (p_1 k_H)/\tilde{s}}{1 + (q_1 k_H)/\tilde{s} + (q_2 k_H^2)/\tilde{s}} \tag{9}$$

$$\gamma_R = \frac{1 + (p_2 k_R/k_V)/\tilde{s}^2 + (p_3 k_R)/\tilde{s}^3 + (p_5 k_R^2/k_V)/\tilde{s}^5 + (p_6 k_R^2)/\tilde{s}^6}{(1 + (p_2 k_R/k_V)/\tilde{s}^2)(1 + (q_1 k_V)/\tilde{s} + (q_3 k_R)/\tilde{s}^3 + (q_4 k_R K_V)/\tilde{s}^4 (q_6 k_R^2)/\tilde{s}^6 + (q_7 K_R^2 k_V)/\tilde{s}^7)} \tag{10}$$

$$\gamma_{SR} = \left[1 + \frac{3(1-2\nu)}{16\pi}\frac{K_H K_V}{\mu K_{SR}}\right]\gamma_H \tag{11}$$

$$\gamma_T = \frac{1 + (p_2 k_T/k_H)/\tilde{s}^2 + (p_3 k_T)/\tilde{s}^3}{(1 + (p_2 k_T/k_H)/\tilde{s}^2)(1 + (q_1 k_H)/\tilde{s} + (q_3 k_T)/\tilde{s}^3 + (q_4 k_H k_T)/\tilde{s}^4)} \tag{12}$$

where $k_V = K_V/(\pi\mu D)$ is the dimensionless vertical stiffness; $k_H = K_H/(\pi\mu D)$ = is the dimensionless horizontal stiffness; $k_R = K_R/(\pi\mu D^3)$ is the dimensionless rocking stiffness; and $k_T = K_T/(\pi\mu D^3)$ is the dimensionless torsional stiffness. Each p and q coefficient is defined in Bordón et al. [44].

The previously defined correction factors allow a partial introduction of foundation–soil–foundation interaction effects, which is only valid when the global response of the rigidly connected foundation system is required. This applies specifically to the jacket structures examined in this study, which include a tie beam.

Finally, the aforementioned is incorporated into a stiffness matrix $\mathrm{K}^{\mathrm{FSFI}}$, which considers the foundation–soil–foundation interaction effects and, similarly to (1), is expressed as follows:

$$\mathbf{K}_0^{\mathrm{FSFI}} = \begin{bmatrix} K_H^{\mathrm{FSFI}} & 0 & 0 & 0 & -K_{SR}^{\mathrm{FSFI}} & 0 \\ 0 & K_H^{\mathrm{FSFI}} & 0 & K_{SR}^{\mathrm{FSFI}} & 0 & 0 \\ 0 & 0.0 & K_V^{\mathrm{FSFI}} & 0 & 0 & 0 \\ 0 & K_{SR}^{\mathrm{FSFI}} & 0 & K_R^{\mathrm{FSFI}} & 0 & 0 \\ -K_{SR}^{\mathrm{FSFI}} & 0 & 0 & 0 & K_R^{\mathrm{FSFI}} & 0 \\ 0 & 0.0 & 0 & 0 & 0 & K_{KT}^{\mathrm{FSFI}} \end{bmatrix} \tag{13}$$

Table 4 shows the values of the single stiffnesses (no-int) and considering the foundation–soil–foundation interaction (FSFI) employed in the study.

Table 4. Stiffness values computed for the single bucket foundations ($K^{\text{no-int}}$) and for the bucket foundations as part of a group, including FSFI (K^{FSFI}).

	$\boldsymbol{K}_{[\,]}^{\text{no-int}}$	$\gamma_{[\,]}$	$\boldsymbol{K}_{[\,]}^{\text{FSFI}}$
Vertical	3.3181×10^{8} [N/m]	0.6525	2.1651×10^{8} [N/m]
Horizontal	4.1424×10^{8} [N/m]	0.5567	2.3061×10^{8} [N/m]
Rocking	6.5522×10^{9} [Nm]	1.0062	6.5928×10^{9} [Nm]
Sway-rocking	1.0540×10^{9} [N]	0.6176	6.5100×10^{8} [N]
Torsional	4.1733×10^{9} [Nm]	0.9819	4.0978×10^{9} [Nm]

3.2. Numerical Model

The numerical tool employed in this study is built upon OpenFAST [60], an advanced open-source multi-physics and multi-fidelity platform developed in Fortran 95, designed for simulating the coupled dynamic behaviour of wind turbines in the time domain. Managed by the National Renewable Energy Laboratory, OpenFAST is not merely a standalone program but rather a comprehensive framework that integrates various computational modules. These modules interact through a loosely coupled time-integration scheme, where a glue code facilitates data exchange between them at each time step.

All time-domain simulations analysed in this study were carried out considering the following features: aerodynamic loads on the blades and tower were computed using the AeroDyn module [61], which incorporates rotor wake and induction effects, blade airfoil aerodynamics, tower influence on fluid behaviour near the blade nodes, and tower drag. Wind input files were generated by TurbSim [62]. The structural dynamic responses of the rotor, drivetrain, nacelle, and tower were modelled with the ElastoDyn module. ServoDyn module is employed for the modelling of the wind turbine's control and electrical subsystems. Wave loads and fluid–structure interaction effects were captured using the HydroDyn module [63], which utilises the potential flow theory, strip theory, or a combination of both to calculate hydrodynamic loads on the submerged portions of the substructure. The structural dynamic response of the substructure, from the transition piece to the foundation, was modelled using the SubDyn module [64], based on a linear frame finite element beam discretisation. Further details on each module can be found in the OpenFAST documentation [60].

In this study, the soil–structure interaction within OpenFAST is modelled using a substructuring approach. The SSI is represented by linear springs connected to the base of the jacket legs. The considered linear spring stiffnesses (see Table 4) represent the main mechanical behaviour of a foundation system of four buckets founded on a homogeneous linear elastic half-space. Such a simple model is reasonable for a first approach to the problem given the small displacements and low frequencies associated with the dynamic response of the system at hand. Other phenomena such as material and radiation damping, soil nonlinearities, soil degradation, and added mass from the foundation system are neglected from the dynamic analysis. If the considered model based on first principles reveals that the FSFI effects are relevant enough, refinements such as these mentioned should be included in future studies.

4. Results

4.1. Frequency Response

Figure 4 presents the fore-aft Power Spectral Densities (PSDs) of the OWT, obtained from fore-aft accelerations measured at the tower top under parked mode conditions and subjected to environmental loads. Results are presented for the three different approaches considered in this study: (a) fixed-base model (labelled No SSI), (b) compliant-base model, without considering FSFI (SSI without FSFI), and (c) compliant-base model, considering FSFI (SSI with FSFI).

The fundamental frequency is 0.31 Hz for the fixed-base scenario, 0.23 Hz when considering SSI without FSFI, and 0.21 Hz when FSFI is taken into account. FSFI plays a

significant role in the reduction of the fundamental frequency, causing approximately a 35% reduction in the fore–aft direction compared to the fixed-base case. These values are in close alignment with those reported by Salem et al. [52] for same the reference jacket structure. It can therefore be assumed that the OpenFAST model accurately represents the dynamic response of the system considering SSI and FSFI. The reduction of the fundamental frequency when considering FSFI may require a refinement of the design to accommodate an additional safety margin, in accordance with DNVGL [65] guidelines.

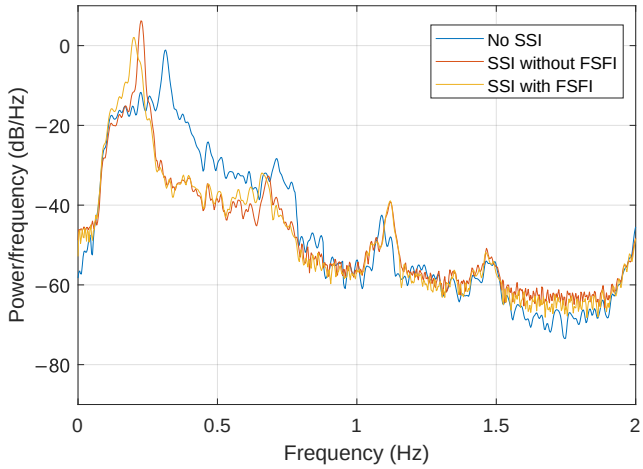

Figure 4. Power Spectral Densities in the fore–aft direction obtained from the response of the 5 MW OWT on the OC4 jacket in parked conditions, under fixed, SSI without FSFI, and SSI with FSFI hypotheses.

4.2. Time History Accelerations

To illustrate the influence of the SSI on the dynamic behaviour of the systems, Figure 5 presents a representative example of the time histories for fore-aft accelerations (0°) at the tower top of the OWT during power production mode. This scenario is subjected to environmental loads aligned with the fore-aft (FA) direction, specifically defined for load cases E-1 and E-2. This variable is relevant because the maximum accelerations in the rotor nacelle assembly (RNA) are limited due to serviceability constraints, and the average amplitude is related to the operational lifespan of the wind turbine.

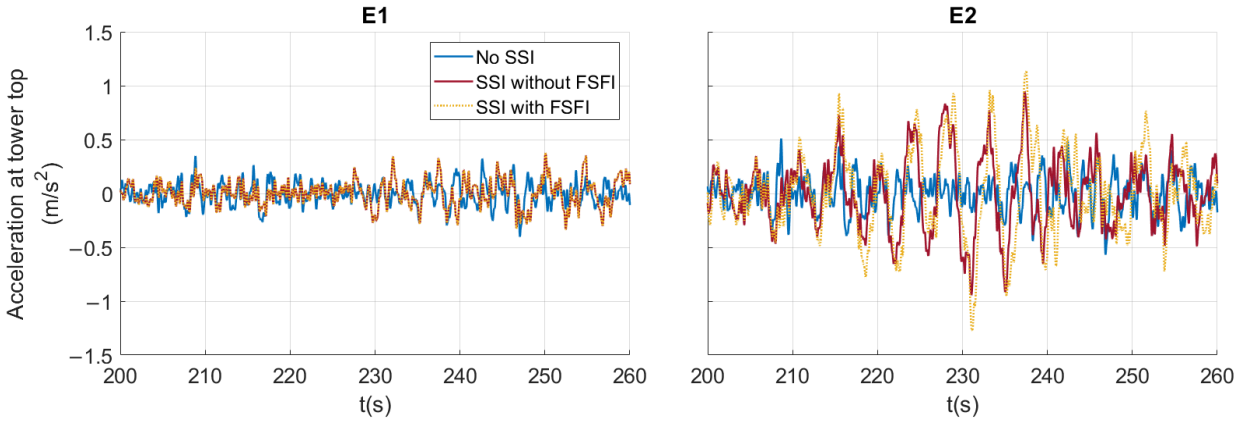

Figure 5. Time history responses corresponding to accelerations at the tower top subjected to environmental loads in the fore-aft direction during power production.

The added flexibility introduced by the foundation leads to amplified peak responses. SSI is critical for the dynamic behaviour of the tower top due to the increased accelerations and displacements observed in this region, particularly when FSFI is taken into account. This highlights the essential role of integrating FSFI to ensure a precise and robust evaluation of wind turbine design. These trends will be explored in more detail in the following subsections.

4.3. Structural Response

The influence of the three different SSI hypotheses in the different load cases is analysed in this section in terms of internal forces in the jacket. In all cases, responses for any given variable are computed as follows:

$$X(t) = \sqrt{X_x(t)^2 + X_y(t)^2} \tag{14}$$

where $X_x(t)$ and $X_y(t)$ are the time histories of the responses along the fore-aft and side-to-side directions, respectively. The results are analysed in terms of peak values and also of root mean squared (RMS) values, which is crucial for determining whether the observed trends are consistent throughout the entire time response, rather than just representative of isolated peaks. A detailed comparison of the results is conducted in terms of bending moments and shear forces at the base of the legs, which connects the foundation to the jacket, specifically at the leg where the maximum force value is obtained, and the tower top accelerations.

Figure 6 illustrates the peak values obtained for each load case and load alignment during power production. Each row shows the accelerations at the top of the tower, the shear forces and the bending moments at the base of the leg, while each column shows the three load cases with their respective load direction configurations. In addition, each coloured bar represents a different SSI hypothesis. As anticipated from Figure 5, accounting for SSI in the system leads to higher peak accelerations at the top of the tower due to the increased flexibility of the system. Increases in peak acceleration of up to 60% are observed between the fixed and SSI with FSFI hypotheses. FSFI reduces peak shear forces while, at the same time, increases peak bending moments. In terms of internal forces, the highest peak values are observed in load case E-2, particularly in scenarios where wave and wind loads are misaligned. The extreme wave loading scenario generates the most significant peak responses in the jacket substructure. However, the maximum acceleration values at the tower top are recorded in load case E-3, corresponding to the extreme wind load scenario. To determine whether the observed trends are consistent throughout the entire time response, Figure 7 presents the shear forces and bending moments at the base of the legs in terms of RMS values, following the same labelling as Figure 6.

The trends in terms of RMS shear forces are similar to those observed for peak shear forces. In terms of bending moments, the RMS values clearly show higher magnitudes when foundation–soil–foundation interaction is considered. This trend is not as evident when bending moments peak values are analysed, where, in some cases, higher values are observed in the fixed-base scenario.

The results indicate that, in terms of RMS values, the internal forces are greater when FSFI is considered, which may have a more significant impact in terms of fatigue. However, when individually analysing each internal force peak value, it can be concluded that the consideration of the FSFI can be either beneficial in terms of shear forces or detrimental in terms of bending moments at the base of the leg. For bending moments, the analysed values correspond to the maximums obtained in the substructure.

After analysing the accelerations and stresses in both peak and RMS values, Figure 8 presents the spectral analysis of the accelerations at the top of the tower, as well as of the shear forces and bending moments obtained at the base of the leg in the load case E-2, specifically when the load directions are aligned at 45 degrees (C45). Each line colour represents the different SSI hypotheses considered in the study. Focusing on the accelerations, it

is clearly observed that the peak value of the first mode decreases when SSI with FSFI is considered, highlighting the significant effect of considering FSFI on the system. Regarding the bending moment, its amplitude is notably affected. Furthermore, while the third mode is observed under fixed-base conditions, it vanishes when SSI and FSFI are taken into account. It is also worth noting that FSFI influences the response of the system along a narrow frequency band that expands, approximately, only between 0.1 and 0.8 Hz. In this range, the response of the model that includes FSFI tends to be slightly higher. However, above this frequency, SSI modifies the response of the compliant system if compared with the fixed-base counterpart, but the additional effect of FSFI is negligible.

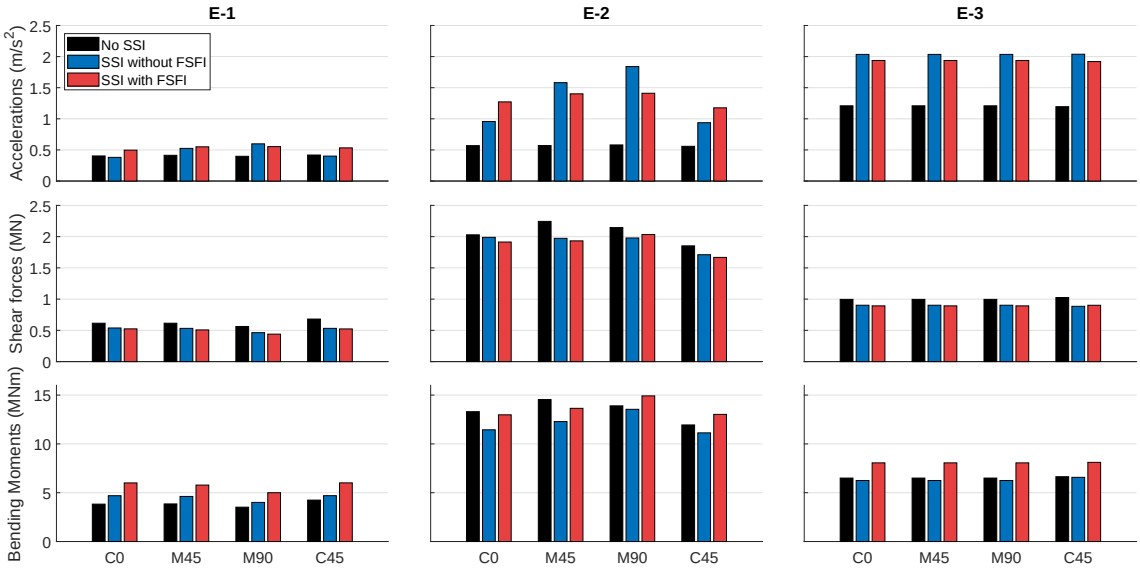

Figure 6. Peak response in terms of accelerations at the tower top, shear forces, and bending moments at the base of the legs for all load cases and SSI hypotheses, during power production. OC4 jacket.

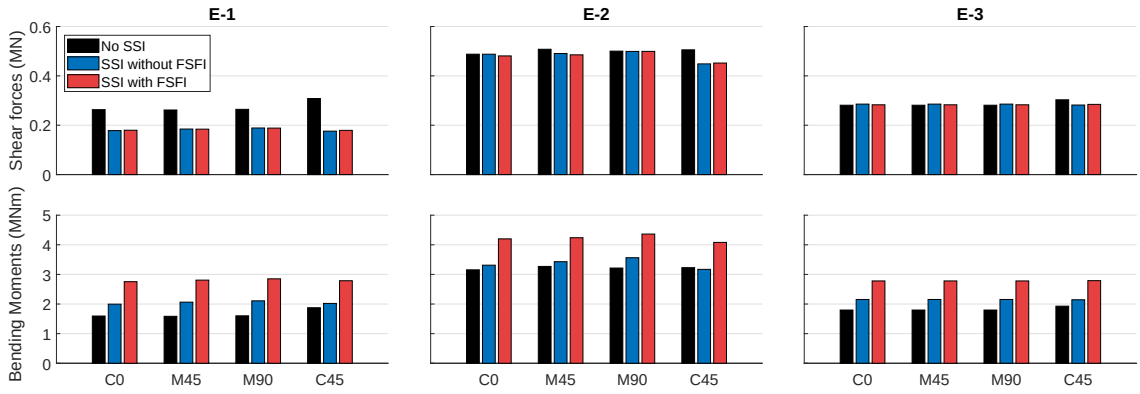

Figure 7. RMS response in terms of shear forces and bending moments at the base of the legs for all load cases and SSI hypotheses, during power production. OC4 jacket.

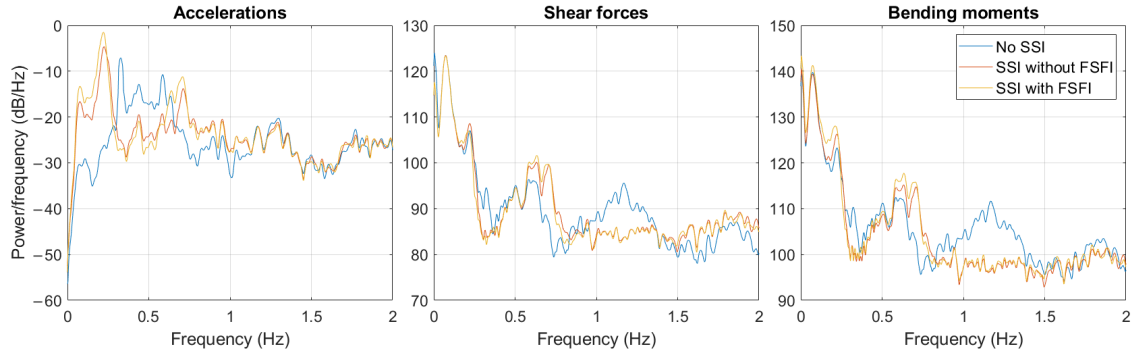

Figure 8. Frequency response for accelerations at the tower top, shear forces, and bending moments at the base of the leg obtained from the OWT on the OC4 jacket in power production, under fixed, SSI without FSFI, and SSI with FSFI hypotheses. Load case E-2. Load direction C45.

4.3.1. Influence of Operational Mode

To evaluate the impact of operational modes on the dynamic behaviour of the jacket supported by buckets, Figure 9 presents the RMS responses of shear forces and bending moments at the base of the legs for the different load cases considered in the study during power production and parked mode conditions. Each row corresponds to a distinct load state, while the vertical axes indicate the load alignments. Square markers denote power production, whereas triangular markers represent the parked mode.

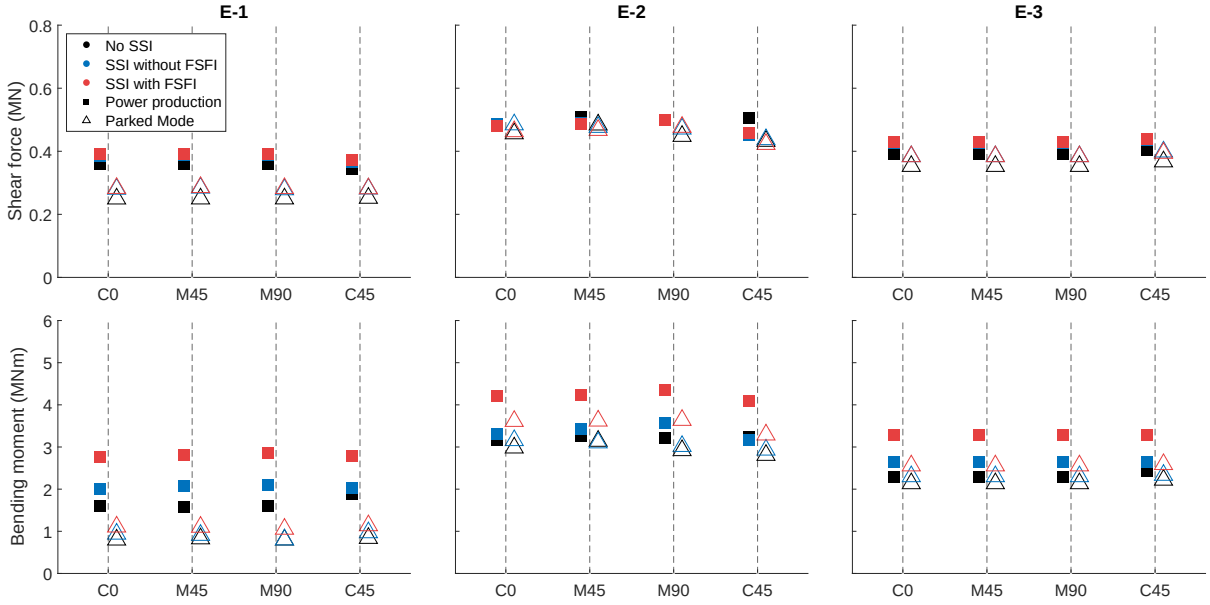

Figure 9. RMS response in terms of shear force and bending moment at the OC4 jacket during both power production and parked modes.

The response computed when FSFI (red markers) is considered tends to generate the highest internal forces, particularly under power production mode in terms of bending moments. However, for shear forces, this trend is less clear, as it varies depending on the specific case and the alignment of the loads. In certain instances, the highest shear forces are recorded when the fixed-base scenario is assumed. In the E-2 load state, smaller differences are observed between the values obtained in the different operational modes, as this scenario is designed to represent an extreme wave load in which aerodynamic influences are less significant. The power production mode is consistently the most unfavourable condition for the internal forces.

4.3.2. Stress Response

This section presents a comparative analysis of the von Mises stresses obtained at the substructure by considering the different SSI hypotheses. Stresses have been evaluated in the critical elements of the jacket, covering the different levels of the structure, including leg and bracing elements.

Figure 10 shows the peak and RMS values (different rows) at the four levels of the jacket (different columns) obtained for case E-2, in which the highest stresses were recorded compared to the other scenarios analysed. The von Mises stresses at the bracing and leg elements are displayed independently, with coloured and grey bars, respectively. Stress values were extracted at different levels of the jacket, allowing for an accurate assessment of the most structurally critical areas and elements. The most unfavourable case, in terms of von Mises stresses, is identified in load case E-2, specifically when the loads are aligned at 45 degrees relative to the position of the jacket.

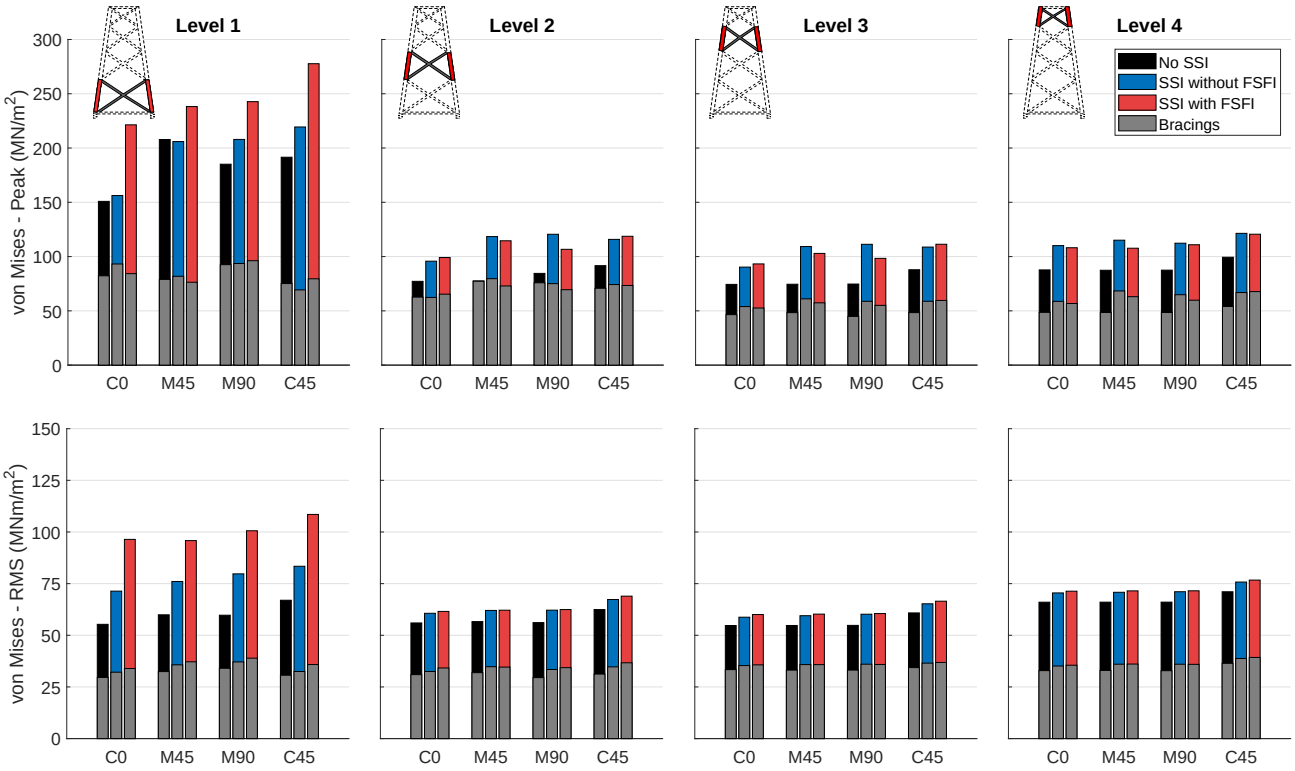

Figure 10. Peak and RMS von Mises stress responses in the OC4 jacket for the different load cases and SSI hypotheses under power production. Coloured bars are used to represent stresses in leg members, and grey bars for stresses in bracing elements.

The areas of the jacket with the highest stresses are located at level 1 of the leg. It is noteworthy that the von Mises stresses at level 2 are similar between the bracing elements and the legs, especially in the fixed-base configuration. Additionally, the bracing elements exhibit relatively uniform stresses across all levels, in contrast to the legs, where significant variations are observed.

The foundation–soil–foundation interaction is clearly significant in terms of von Mises stresses. Unlike what happens in terms of internal forces, in most cases, the maximum stresses occur when the group effect is considered, underscoring its relevance in the dynamic response analysis of jackets. This phenomenon is observed not only in peak responses but also in RMS values. In particular, in terms of peak values, a difference of up to 31% has been recorded when comparing cases that consider SSI with FSFI against those that do not, and a 13% difference between the fixed-base model and the model considering SSI without FSFI at the leg (level 1).

4.4. Impact of Jacket Design on Group Effect Influence in the Dynamic Response

The results presented above demonstrated that the structural responses of a specific jacket, including accelerations, internal forces, and stresses, vary significantly with the characteristics of soil–structure interaction. However, an important question arises: how do structural responses change if the jacket design is modified while external conditions remain constant?

To address this question, the response of a slightly different jacket structure is now analysed. To do so, the optimised structure computed by Couceiro et al. [66] is considered. Figure 11 shows the geometry of the optimised jacket. This choice enables a detailed comparison with the reference jacket, evaluating how variations in the SSI modelling affect structural responses under the same loading conditions. Furthermore, an analysis of the variations between both jackets will be included, highlighting the differences and similarities in structural behaviour, thus providing a comprehensive understanding of the effects of changing the jacket design.

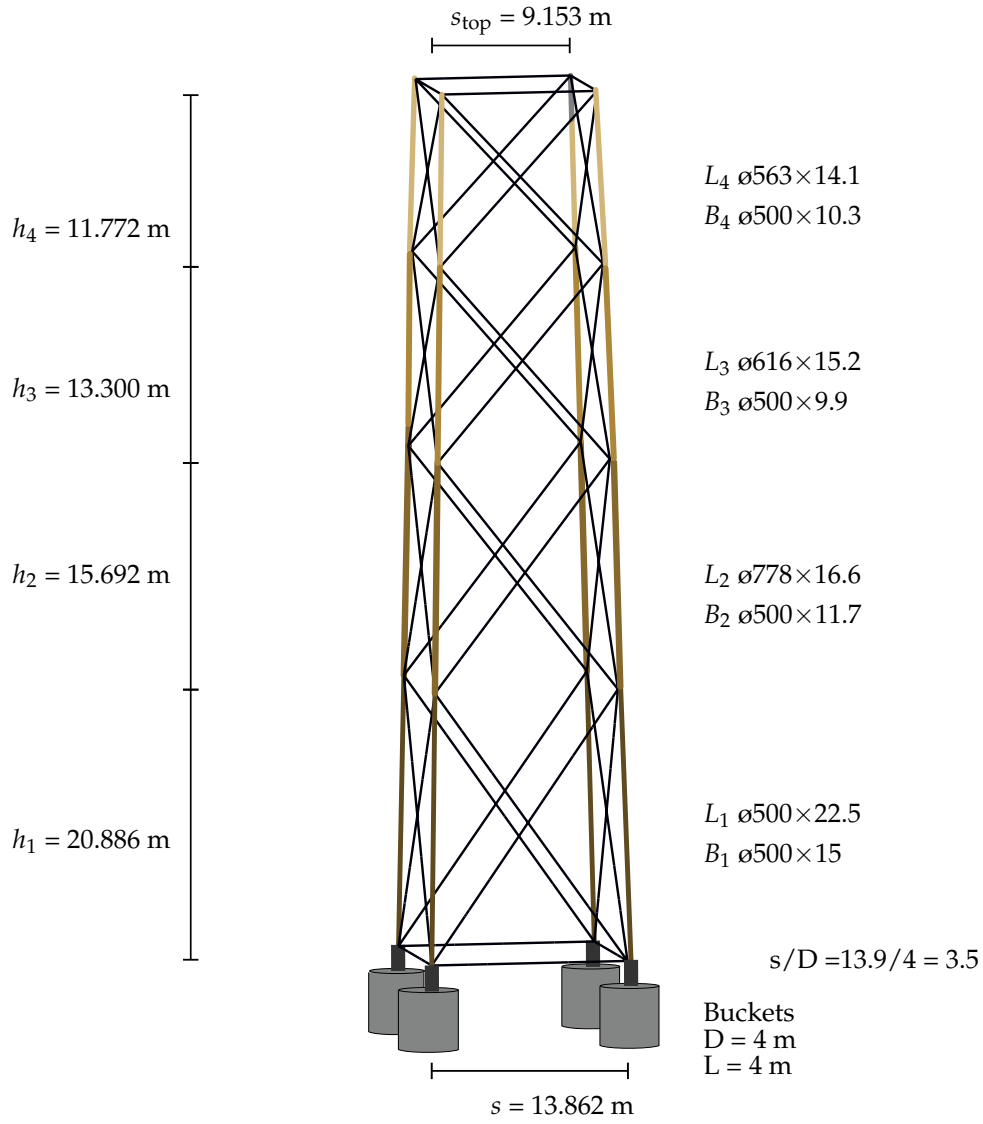

Figure 11. Geometry of the optimised jacket with buckets. The diameter and thickness of each leg level L_i and bracings B_i are provided at the right of the figure in millimetres.

Figure 12 shows the fore-aft PSDs of the offshore wind turbine mounted on the two different jackets, obtained from fore-aft accelerations measured at the tower top under parked conditions and environmental loads in the three different SSI scenarios.

The fundamental frequencies obtained for the optimised jacket are consistent with those presented by Couceiro et al. [66]. Table 5 summarises the fundamental frequency of the system under the three different modelling approaches. The consideration of FSFI significantly reduces the values of the first three natural frequencies, with reductions of approximately 35% and 20% in the fore-aft fundamental frequency for the original and optimised jackets, respectively.

It is important to highlight that the optimised structure was designed neglecting SSI, with a natural frequency closely aligned with the 1P frequency. As such, this design may be unsuitable for the proposed bucket foundation and soil parameters.

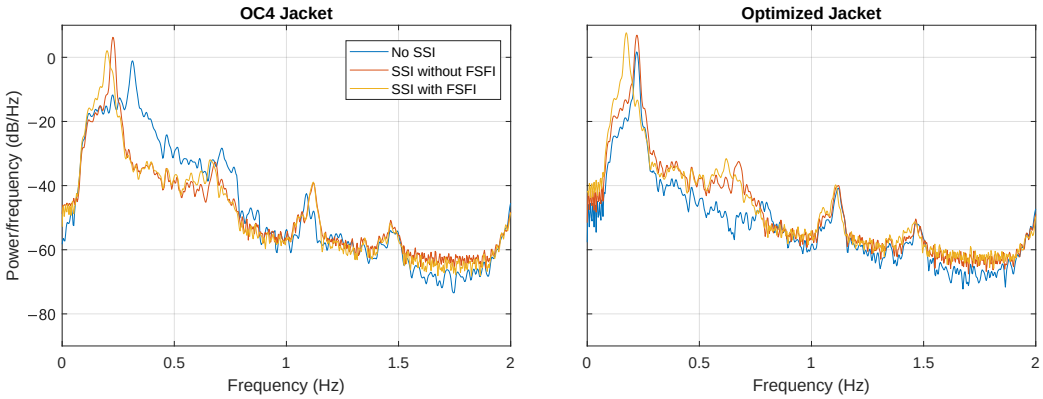

Figure 12. Power Spectral Densities in the fore–aft direction obtained from the response of the 5MW OWT on the OC4 jacket and of the optimised jacket in parked conditions, under fixed, SSI without FSFI, and SSI with FSFI hypotheses.

Table 5. OWT fundamental frequencies.

	Reference Jacket	Optimised Jacket
No SSI, fore-aft	0.314 Hz (3.18 s)	0.222 Hz (4.50 s)
SSI without FSFI, fore-aft	0.228 Hz (4.39 s)	0.220 Hz (4.55 s)
SSI with FSFI, fore-aft	0.205 Hz (4.88 s)	0.180 Hz (5.56 s)

Figure 13 shows the peak values of accelerations at the tower top, as well as the shear forces and bending moments at the base of the legs for the optimised jacket. These values are provided for the different SSI configurations and for each load case and load alignment considered. Each coloured bar represents the results obtained for the models that consider fixed-base condition (no SSI), SSI using the corresponding stiffnesses to the single foundations (SSI without FSFI), and FSFI (SSI with FSFI). On the other hand, Figure 14 displays the RMS values for shear forces and bending moments, thus enabling a comparison with the peak values and an assessment of the consistency of the observed trends.

The trends in accelerations and bending moments are similar to those observed in the original jacket, where the highest peak values occur when SSI is included, particularly when FSFI is considered. However, the trends in shear forces exhibit an increase towards the FSFI, particularly in E-2 and E-3, in contrast to the original OC4 jacket. In addition, in comparison to the original jacket, the RMS values present a correlation between the trends in both internal forces, although the differences in RMS shear forces values in the different SSI hypotheses are less pronounced.

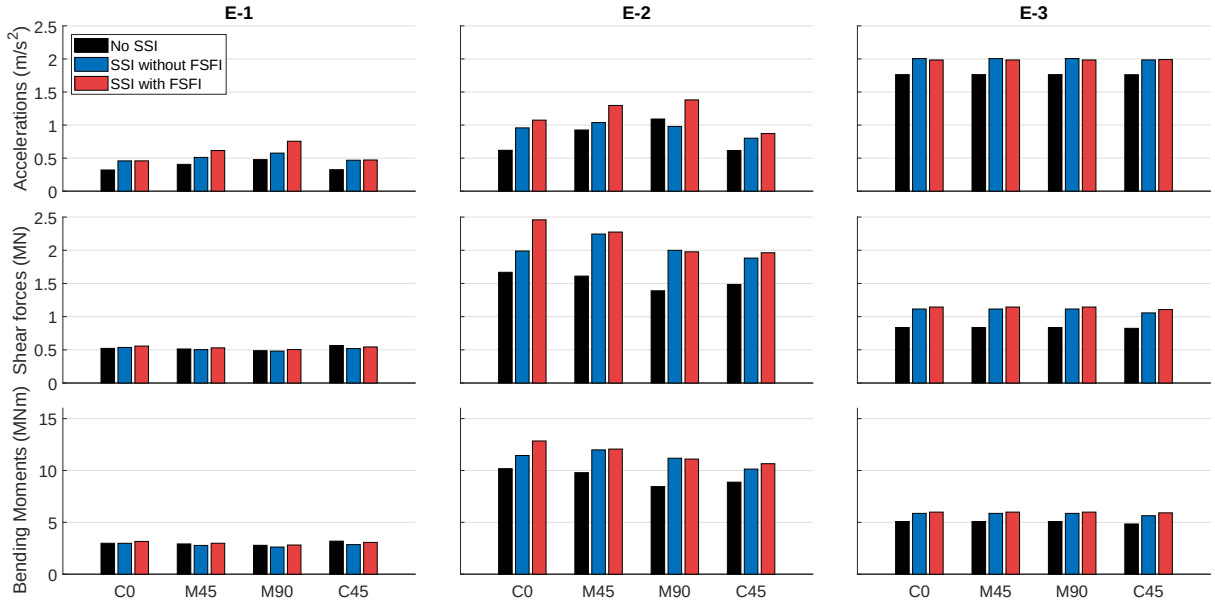

Figure 13. Peak response in terms of accelerations at the tower top, shear forces, and bending moments at the base of the legs for all load cases and SSI hypotheses, during power production. Optimised jacket.

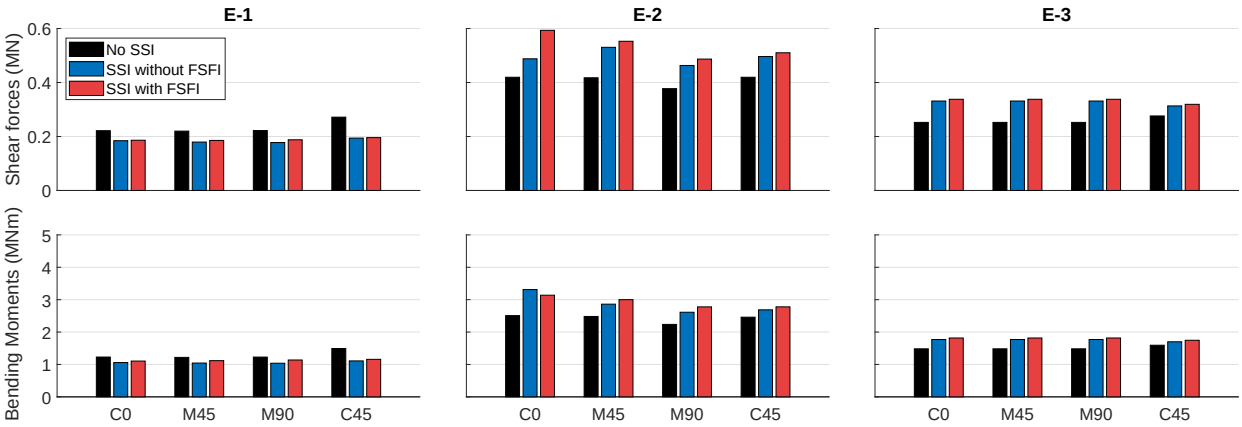

Figure 14. RMS response in terms of shear forces and bending moments at the base of the legs for all load cases and SSI hypotheses, during power production. Optimised jacket.

It is crucial to emphasise that the optimised jacket experiences higher peak accelerations, shear forces, and bending moments when soil–structure interaction (either considering FSFI or not) is considered, compared to the fixed-base scenario. This trend is consistent across all analysed cases. However, this behaviour is not observed in the shear forces of the reference jacket.

Finally, Figure 15 presents the peak and RMS response in terms of von Mises stresses at the different levels of the jacket substructure, for the E-2 case. The von Mises stresses are shown with coloured bars for the legs and grey bars for the bracing elements.

The results are largely similar to those obtained in the reference jacket. The highest peak stress areas are located at levels 1 and 4 of the leg. Additionally, the bracing elements demonstrate relatively uniform stresses across all levels, in contrast to the legs, where significant variations are observed. The maximum stresses occur when wind and waves loads are aligned at 45°. The difference in peak values is approximately 8% higher when comparing SSI with FSFI to SSI without FSFI. In contrast, for the OC4 jacket, this difference is notably larger, at approximately 21% when FSFI is considered. However, in the optimised

jacket, smaller differences in RMS values are observed when considering the different SSI hypotheses, in contrast to the reference jacket, where the FSFI notably increased the RMS values. Moreover, with regard to the RMS values, von Mises stresses across the different leg levels are more similar. It is noteworthy that the maximum RMS value is not observed at level 1, as in the original jacket. This highlights the significance of the different SSIs on each jacket individually, indicating that the influence of FSFI in each jacket must be thoroughly analysed.

It is important to emphasise that the optimised jacket was designed assuming fixed-base hypothesis [66]. However, when considering soil–structure interaction, the observed reduction in natural frequency and the increase in von Mises stresses indicate that the jacket structure becomes unsuitable for the loading conditions analysed in this study.

After comparing the influence of considering the bucket–soil–bucket interaction in different substructures, distinct behaviours are observed in both jackets. In terms of individual internal forces, the SSI exhibits variable behaviours depending on the jacket, highlighting the importance of analysing SSI in the performance of each substructure for the same wind turbine. This effect significantly depends on the natural frequencies of the system and the dynamic loads. Therefore, the relevance of studying the effects of SSI on the dynamic behaviour of each specific jacket becomes evident.

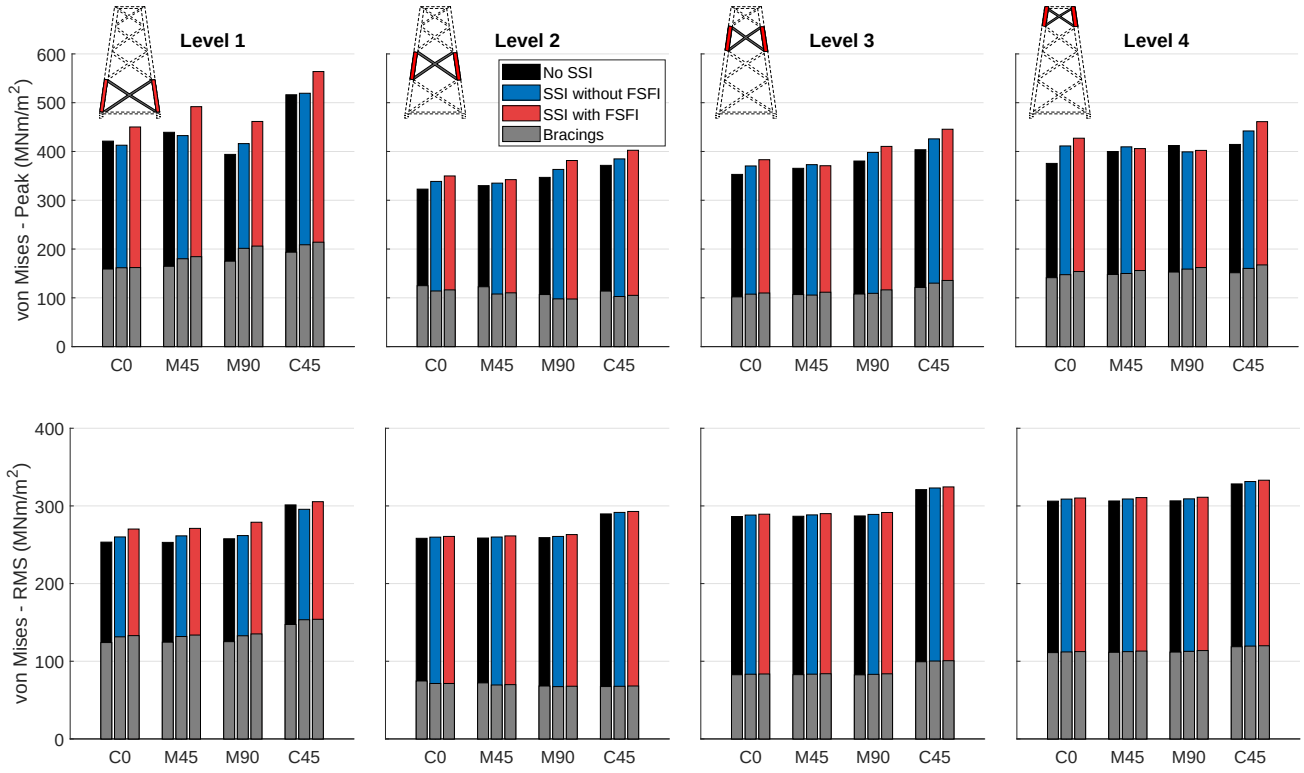

Figure 15. Peak and RMS von Mises stress responses in the optimised jacket for the different load cases and SSI hypotheses under power production. Coloured bars are used to represent stresses in leg members, and grey bars for stresses in bracing elements.

5. Discussion

Foundation–soil–foundation interaction (FSFI) has been shown to produce significant effects on the dynamic response of the system. First, the influence of soil–structure interaction (SSI) is more pronounced in the reference jacket, where a 35% reduction in natural frequency is noted. In contrast, in the optimised jacket, the reduction is significantly less pronounced as a consequence of the increased flexibility of the system. Nevertheless, in both cases, the incorporation of the FSFI leads to a decrease in natural frequency, which is consistent with previous studies, such as those by Salem et al. [52] and Bordón et al. [44].

Moreover, in the optimised jacket, whose natural frequency is already close to the 1P rotor frequency, the additional reduction caused by SSI leads to the natural frequency falling to values unsuitable for the wind turbine design. Consequently, it can be concluded that incorporating the SSI effect in the design and optimisation process of jackets is essential to ensure adequate structural performance and prevent resonance issues.

In regard to accelerations and displacements, the consideration of SSI and FSFI results in an increase in peak values. This increase can have significant implications for the nacelle components, potentially affecting the service life of the OWT. The increase in accelerations results in higher dynamic demands on the structure, which could accelerate fatigue processes in critical components, further highlighting the importance of incorporating these effects in the design and analysis of the OWT jacket.

SSI induces significant variations in the different internal forces analysed at the foundation. The authors can conclude that SSI and FSFI can have both positive and negative impacts on the analysis of internal forces in the jacket structure. Therefore, it is crucial to conduct a detailed SSI analysis for each jacket design, as the structural behaviour can vary significantly depending on the specific conditions.

Based on the results obtained by comparing different operating modes, the power production mode is consistently the most unfavourable condition for the internal forces in the substructure. However, in some of the analysed load cases, the obtained results showed smaller differences. Therefore, it is recommended that the dynamic response be analysed on a case-by-case basis.

Considering FSFI produces the most unfavourable results in terms of stresses, particularly when the stresses align at 45° relative to the jacket's orientation. This behaviour is not explicitly detailed in current standards, which is understandable in the case of monopiles due to their cylindrical symmetry. However, in jacket substructures, this effect causes a significant increase in stresses, highlighting the importance of considering this phenomenon in foundation design. The highest stresses consistently concentrate in the lower part of the jacket, specifically at level 1, particularly in the legs. This behaviour is observed across all load conditions and for both jackets analysed.

6. Conclusions

This study has investigated the influence of foundation–soil–foundation interaction on the dynamic behaviour of jacket substructures founded on buckets for offshore wind turbines. A parametric analysis was conducted, incorporating critical load cases identified for conservative foundation design, as outlined by Jalbi et al. [55] for jacket structures. The study considered four different load configurations, including collinear wind and wave loads, as well as misaligned cases at 45° and 90°, providing a comprehensive assessment of the varying loading directions. The dynamic response of the system was evaluated in terms of key structural parameters, such as, bending moments, shear forces, and stresses on the jacket substructure. In order to evaluate the influence of FSFI on different substructure configurations, simulations were performed considering the NREL 5MW OWT mounted on the jacket defined in the OC4 project, and a comparative analysis employed an optimised jacket. The dynamic response was analysed with an OpenFAST model that incorporated soil–structure interaction and accounted for the presence of multi-bucket foundations for a homogeneous soil profile.

It was found that foundation–soil–foundation interaction can play a role in increasing the magnitude of the structural response in terms not only of accelerations but, more importantly, in terms of shear forces, bending moments, and stresses in many different situations. In other words, ignoring the influence of the interaction between nearby foundations (as is usually assumed in the analysis of this systems) may contribute to underestimating the structural response of the jacket. One of the reasons that explains this influence of foundation–soil–foundation interaction over the structural response is the changes produced in the fundamental frequency of the structure: foundation–soil–foundation interaction modifies the stiffnesses of each individual foundation in the group (the well-known

group effect of the foundations) and, given that the modes and natural frequencies of the whole system depend on such stiffnesses, they are also modified. In turn, if modes and natural frequencies change, the structural response of every element is also affected.

Therefore, even though additional future work is still needed for the development of more elaborated models that include the aspects that have been disregarded in this first study, the authors recommend considering the effects of foundation–soil–foundation interaction in the analysis and design processes of jacket support structures for OWTs.

Author Contributions: Conceptualisation, C.R.-S. and L.A.P.; methodology, C.R.-S., L.A.P. and J.D.R.B.; software, C.R.-S.; validation, C.R.-S.; formal analysis, C.R.-S. and L.A.P.; investigation, C.R.-S., L.A.P. and J.D.R.B.; resources, L.A.P.; data curation, C.R.-S.; writing—original draft preparation, C.R.-S.; writing—review and editing, L.A.P. and J.D.R.B.; visualisation, C.R.-S.; supervision, L.A.P.; project administration, L.A.P.; funding acquisition, C.R.-S. and L.A.P. All authors have read and agreed to the published version of the manuscript.

Funding: This research was funded by the Agencia Estatal de Investigación and the Ministerio de Ciencia, Innovación y Universidades of Spain (MCIN/AEI/10.13039/501100011033) through Research Project PID2020-120102RB-I00 and predoctoral research fellowship TESIS2022010011 (C. Romero-Sanchez) from the Consejería de Universidades, Ciencia e Innovación y Cultura, and by the European Social Fund Plus (ESF+).

Institutional Review Board Statement: Not applicable.

Informed Consent Statement: Not applicable.

Data Availability Statement: The data that support the findings of this study are available from the corresponding author upon reasonable request.

Conflicts of Interest: The authors declare no conflicts of interest.

Abbreviations

The following abbreviations are used in this manuscript:

OWT	Offshore wind turbine
SSI	Soil–structure interaction
FSFI	Foundation–soil–foundation interaction
FEM	Finite Element Method
BEM	Boundary Element Method
D	Diameter of the bucket
L	Length of the bucket
ν	Poisson's ratio of the soil
μ	Shear modulus of the soil
K_0^{no-int}	Stiffness matrix without considering foundation–soil–foundation interaction
K_0^{int}	Stiffness matrix considering foundation–soil–foundation interaction
$\tilde{s}$	Dimensionless spacing (distance) between closest foundations (polygonal arrangement)
γ	Group effect stiffness correction factor
V_r	Rated wind speed
H_{jacket}	Height jacket
H_{top}	Height hub from mean sea level
W	Height water
s_{top}	Spacing jacket top
s	Spacing jacket bottom
DLCs	Design Load Cases
NTM	Normal Turbulence Model
ETM	Extreme Turbulence Model
EOG	Extreme Operating Gust
ESS	Extreme Sea States
EWH	Extreme Wave Height
C0	Wind and waves loads are collinear (0°)

M90	Wind and waves loads are misalignment by 90°
M45	Wind and waves loads are misalignment by 45°
C45	Wind and waves loads act at 45° relative to the structure
H_S	Significant wave height
T_S	Significant wave period
H_m	Maximum wave height
T_m	Maximum wave period

References

1. Council, G.W.E. *Global Offshore Wind Report 2024*; Technical Report; GWEC: Brussels, Belgium, 2024.
2. McCoy, A.; Musial, W.; Hammond, R.; Mulas Hernando, D.; Duffy, P.; Beiter, P.; Perez, P.; Baranowski, R.; Reber, G.; Spitsen, P. *Offshore Wind Market Report: 2024 Edition*; Technical Report; National Renewable Energy Laboratory (NREL): Golden, CO, USA, 2024.
3. Zania, V. Natural vibration frequency and damping of slender structures founded on monopiles. *Soil Dyn. Earthq. Eng.* **2014**, *59*, 8–20. [CrossRef]
4. Damgaard, M.; Zania, V.; Andersen, L.V.; Ibsen, L.B. Effects of soil–structure interaction on real time dynamic response of offshore wind turbines on monopiles. *Eng. Struct.* **2014**, *75*, 388–401. [CrossRef]
5. Álamo, G.; Aznárez, J.; Padrón, L.; Martínez-Castro, A.; Gallego, R.; Maeso, O. Dynamic soil-structure interaction in offshore wind turbines on monopiles in layered seabed based on real data. *Ocean Eng.* **2018**, *156*, 14–24. [CrossRef]
6. Medina, C.; Álamo, G.; Quevedo-Reina, R. Evolution of the seismic response of monopile-supported offshore wind turbines of increasing size from 5 to 15 MW including dynamic soil-structure interaction. *J. Mar. Sci. Eng.* **2021**, *9*, 1285. [CrossRef]
7. Li, W.; Li, X.; Zhao, X.; Yin, Q.; Zhu, M.; Yang, L. The Method of the Natural Frequency of the Offshore Wind Turbine System Considering Pile–Soil Interaction. *J. Mar. Sci. Eng.* **2024**, *12*, 1912. [CrossRef]
8. Abdullahi, A.; Wang, Y.; Bhattacharya, S. Comparative modal analysis of monopile and jacket supported offshore wind turbines including soil-structure interaction. *Int. J. Struct. Stab. Dyn.* **2020**, *20*, 2042016. [CrossRef]
9. Abhinav, K.; Saha, N. Coupled hydrodynamic and geotechnical analysis of jacket offshore wind turbine. *Soil Dyn. Earthq. Eng.* **2015**, *73*, 66–79. [CrossRef]
10. Quevedo-Reina, R.; Álamo, G.; Aznárez, J. Global Sensitivity Analysis of the Fundamental Frequency of Jacket-Supported Offshore Wind Turbines Using Artificial Neural Networks. *J. Mar. Sci. Eng.* **2024**, *12*, 2011. [CrossRef]
11. Arany, L.; Bhattacharya, S.; Macdonald, J.H.; Hogan, S.J. Closed form solution of Eigen frequency of monopile supported offshore wind turbines in deeper waters incorporating stiffness of substructure and SSI. *Soil Dyn. Earthq. Eng.* **2016**, *83*, 18–32. [CrossRef]
12. Jalbi, S.; Bhattacharya, S. Closed form solution for the first natural frequency of offshore wind turbine jackets supported on multiple foundations incorporating soil-structure interaction. *Soil Dyn. Earthq. Eng.* **2018**, *113*, 593–613. [CrossRef]
13. Kaynia, A.M.; Kausel, E. Dynamics of piles and pile groups in layered soil media. *Soil Dyn. Earthq. Eng.* **1991**, *10*, 386–401. [CrossRef]
14. Padrón, L.; Aznárez, J.; Maeso, O. BEM–FEM coupling model for the dynamic analysis of piles and pile groups. *Eng. Anal. Bound. Elem.* **2007**, *31*, 473–484. [CrossRef]
15. Carbonari, S.; Morici, M.; Dezi, F.; Gara, F.; Leoni, G. Soil-structure interaction effects in single bridge piers founded on inclined pile groups. *Soil Dyn. Earthq. Eng.* **2017**, *92*, 52–67. [CrossRef]
16. Latini, C.; Zania, V. Dynamic lateral response of suction caissons. *Soil Dyn. Earthq. Eng.* **2017**, *100*, 59–71. [CrossRef]
17. Bordón, J.; Aznárez, J.; Maeso, O. Dynamic model of open shell structures buried in poroelastic soils. *Comput. Mech.* **2017**, *60*, 269–288. [CrossRef]
18. Latini, C.; Zania, V. Vertical dynamic impedance of suction caissons. *Soils Found.* **2019**, *59*, 1113–1127. [CrossRef]
19. He, R.; Kaynia, A.M. Dynamic impedances and load carrying mechanism for skirted foundations. *Mar. Struct.* **2021**, *79*, 103023. [CrossRef]
20. Gazetas, G. Formulas and charts for impedances of surface and embedded foundations. *J. Geotech. Eng.* **1991**, *117*, 1363–1381. [CrossRef]
21. Doherty, J.; Deeks, A. Elastic response of circular footings embedded in a non-homogeneous half-space. *Géotechnique* **2003**, *53*, 703–714. [CrossRef]
22. *Offshore Standard DNV-OS-J101*; Design of Offshore Wind Turbine Structures. DNV: Bærum, Norway; DetNorske Veritas AS: Shenzhen, China, 2014.
23. Wong, H.; Luco, J. Dynamic interaction between rigid foundations in a layered half-space. *Soil Dyn. Earthq. Eng.* **1986**, *5*, 149–158. [CrossRef]
24. Dobry, R.; Gazetas, G. Simple method for dynamic stiffness and damping of floating pile groups. *Geotechnique* **1988**, *38*, 557–574. [CrossRef]
25. Zhong, M.; Meng, K. Dynamic Interaction Factor of Pipe Group Piles Considering the Scattering Effect of Passive Piles. *J. Mar. Sci. Eng.* **2023**, *11*, 1698. [CrossRef]
26. Reumers, P.; Lombaert, G.; Degrande, G. The effect of foundation–soil–foundation interaction on the response of continuous, multi-span railway bridges. *Eng. Struct.* **2024**, *299*, 117096. [CrossRef]

27. Zeolla, E.; de Silva, F.; Sica, S. Towards a practice-oriented procedure to account for static and dynamic interaction among three adjacent shallow foundations. *Comput. Geotech.* **2024**, *170*, 106242. [CrossRef]
28. Karabalis, D.L.; Mohammadi, M. 3-D dynamic foundation-soil-foundation interaction on layered soil. *Soil Dyn. Earthq. Eng.* **1998**, *17*, 139–152. [CrossRef]
29. Chen, L. Dynamic interaction between rigid foundations on multi-layered stratum. *J. Earthq. Eng.* **2016**, *20*, 505–534. [CrossRef]
30. Zeolla, E.; de Silva, F.; Sica, S. A simplified approach to account for through-soil interaction between two adjacent shallow foundations. *Bull. Earthq. Eng.* **2023**, *21*, 2503–2532. [CrossRef]
31. Aji, H.D.; Heiland, T.; Wuttke, F.; Stark, A.; Dineva, P. Dynamic impedance and compliance surfaces of twin adjacent surface foundations under synchronous and asynchronous loads. *Soil Dyn. Earthq. Eng.* **2024**, *182*, 108740. [CrossRef]
32. Alati, N.; Failla, G.; Arena, F. Seismic analysis of offshore wind turbines on bottom-fixed support structures. *Philos. Trans. R. Soc. A Math. Phys. Eng. Sci.* **2015**, *373*, 20140086. [CrossRef]
33. Abhinav, K.; Saha, N. Nonlinear dynamical behaviour of jacket supported offshore wind turbines in loose sand. *Mar. Struct.* **2018**, *57*, 133–151. [CrossRef]
34. Romero-Sánchez, C.; Padrón, L. Influence of wind and seismic ground motion directionality on the dynamic response of four-legged jacket-supported Offshore Wind Turbines. *Eng. Struct.* **2024**, *300*, 117191. [CrossRef]
35. Ju, S.H.; Huang, Y.C. Analyses of offshore wind turbine structures with soil-structure interaction under earthquakes. *Ocean Eng.* **2019**, *187*, 106190. [CrossRef]
36. James, M.; Haldar, S. Seismic vulnerability of jacket supported large offshore wind turbine considering multidirectional ground motions. *Structures* **2022**, *43*, 407–423. [CrossRef]
37. Bhattacharya, S.; Nikitas, N.; Garnsey, J.; Alexander, N.; Cox, J.; Lombardi, D.; Wood, D.M.; Nash, D.F. Observed dynamic soil–structure interaction in scale testing of offshore wind turbine foundations. *Soil Dyn. Earthq. Eng.* **2013**, *54*, 47–60. [CrossRef]
38. Jalbi, S.; Nikitas, G.; Bhattacharya, S.; Alexander, N. Dynamic design considerations for offshore wind turbine jackets supported on multiple foundations. *Mar. Struct.* **2019**, *67*, 102631. [CrossRef]
39. Plodpradit, P.; Kwon, O.; Dinh, V.N.; Murphy, J.; Kim, K.D. Suction bucket pile–soil–structure interactions of offshore wind turbine jacket foundations using coupled dynamic analysis. *J. Mar. Sci. Eng.* **2020**, *8*, 416. [CrossRef]
40. Antoniou, M.; Kourkoulis, R.; Gelagoti, F.; Anastasopoulos, I. Simplified method for performance-based seismic design of suction caissons supporting jacket offshore wind turbines. *Soil Dyn. Earthq. Eng.* **2022**, *155*, 107169. [CrossRef]
41. Cheng, Y.; Luo, Y.; Wang, J.; Dai, K.; Wang, W.; El Damatty, A. Fragility and vulnerability development of offshore wind turbines under aero-hydro loadings. *Eng. Struct.* **2023**, *293*, 116625. [CrossRef]
42. Zhang, B.; Liu, R.; Wang, L.; Wang, X.; Wang, L.; Li, W.; Hong, Y. Cyclic response and load transfer mechanism of suction bucket jackets supporting offshore wind turbines in soft clay. *Ocean Eng.* **2024**, *313*, 119135. [CrossRef]
43. Zhu, H.; Lian, J.; Guo, Y.; Wang, H. A Numerical Model for the Scour Effect on the Bearing Capacity of an Offshore Wind Turbine with a Five-Bucket Jacket Foundation. *J. Mar. Sci. Eng.* **2024**, *12*, 753. [CrossRef]
44. Bordón, J.D.R.; Aznárez, J.J.; Maeso, O.; Bhattacharya, S. Simple approach for including foundation–soil–foundation interaction in the static stiffnesses of multi-element shallow foundations. *Géotechnique* **2021**, *71*, 686–699. [CrossRef]
45. Wei, K.; Myers, A.T.; Arwade, S.R. Dynamic effects in the response of offshore wind turbines supported by jackets under wave loading. *Eng. Struct.* **2017**, *142*, 36–45. [CrossRef]
46. Liang, F.; Yuan, Z.; Liang, X.; Zhang, H. Seismic response of monopile-supported offshore wind turbines under combined wind, wave and hydrodynamic loads at scoured sites. *Comput. Geotech.* **2022**, *144*, 104640. [CrossRef]
47. Mroczek, M.M.; Arwade, S.R.; Lackner, M.A. Design optimization of offshore wind jacket piles by assessing support structure orientation relative to metocean conditions. *Wind Energy Sci. Discuss.* **2023**, *2023*, 807–817. . [CrossRef]
48. Sun, M.; Shan, Z.; Wang, W.; Xu, S.; Liu, X.; Zhang, H.; Guo, X. Numerical Investigation into the Stability of Offshore Wind Power Piles Subjected to Lateral Loads in Extreme Environments. *J. Mar. Sci. Eng.* **2024**, *12*, 915. [CrossRef]
49. Padrón, L.; Carbonari, S.; Dezi, F.; Morici, M.; Bordón, J.; Leoni, G. Seismic response of large offshore wind turbines on monopile foundations including dynamic soil–structure interaction. *Ocean Eng.* **2022**, *257*, 111653. [CrossRef]
50. Jonkman, J.; Butterfield, S.; Musial, W.; Scott, G. *Definition of a 5-MW Reference Wind Turbine for Offshore System Development*; Technical Report; National Renewable Energy Lab. (NREL): Golden, CO, USA, 2009.
51. Vorpahl, F.; Popko, W.; Kaufer, D. *Description of a Basic Model of the "UpWind reference Jacket" for Code Comparison in the OC4 Project Under IEA Wind Annex XXX*; Fraunhofer Institute for Wind Energy and Energy System Technology (IWES): Bremerhaven, Germany, 2011; Volume 450.
52. Salem, A.; Jalbi, S.; Bhattacharya, S. Vertical stiffness functions of rigid skirted caissons supporting offshore wind turbines. *J. Mar. Sci. Eng.* **2021**, *9*, 573. [CrossRef]
53. *Offshore Standard DNV-ST-0437*; Loads and Site Conditions for Wind Turbines. DNV: Bærum, Norway; DetNorske Veritas AS: Shenzhen, China, 2016.
54. *IEC 61400-1:2020*; Wind Energy Generation Systems—Part 1: Design Requirements. International Electrotechnical Commission: London, UK, 2020.
55. Jalbi, S.; Bhattacharya, S. Concept design of jacket foundations for offshore wind turbines in 10 steps. *Soil Dyn. Earthq. Eng.* **2020**, *139*, 106357. [CrossRef]

56. Romero-Sánchez, C.; Padrón, L.A. Seismic response of jacket-supported offshore wind turbines for different operational modes considering earthquake directionality. *Ocean Eng.* **2024**, *311*, 118798. [CrossRef]
57. Meng, J.; Dai, K.; Zhao, Z.; Mao, Z.; Camara, A.; Zhang, S.; Mei, Z. Study on the aerodynamic damping for the seismic analysis of wind turbines in operation. *Renew. Energy* **2020**, *159*, 1224–1242. [CrossRef]
58. Bordón, J.; Aznárez, J.; Padrón, L.; Maeso, O.; Bhattacharya, S. Closed-form stiffnesses of multi-bucket foundations for OWT including group effect correction factors. *Mar. Struct.* **2019**, *65*, 326–342. [CrossRef]
59. Wolf, J.P.; Deeks, A.J. *Foundation Vibration Analysis: A Strength of Materials Approach*; Elsevier: Amsterdam, The Netherlands, 2004.
60. National Renewable Energy Laboratory. OpenFAST Documentation. Release v3.5.2. 2024. Available online: https://openfast.readthedocs.io/en/main/ (accessed on 1 October 2024).
61. Moriarty, P.; Hansen, A. *AeroDyn Theory Manual*; Technical Report; National Renewable Energy Lab.: Golden, CO, USA, 2005.
62. Jonkman, B. *TurbSim User's Guide: Version 1.50*; Technical Report; National Renewable Energy Lab. (NREL): Golden, CO, USA, 2009.
63. Jonkman, J.M.; Robertson, A.; Hayman, G.J. *HydroDyn User's Guide and Theory Manual*; National Renewable Energy Laboratory: Golden, CO, USA, 2014.
64. Damiani, R.; Jonkman, J.; Hayman, G. *SubDyn User's Guide and Theory Manual*; Technical Report; National Renewable Energy Lab. (NREL): Golden, CO, USA, 2015.
65. Dnv, G. *Offshore Soil Mechanics and Geotechnical Engineering (DNVGL-RP-C212)*; DNV: Bærum, Norway, 2017.
66. Couceiro, I.; París, J.; Navarrina, F.; Guizán, R.; Colominas, I. Optimization of offshore steel jackets: Review and proposal of a new formulation for time-dependent constraints. *Arch. Comput. Methods Eng.* **2020**, *27*, 1049–1069. [CrossRef]